JACS
JOURNAL OF THE AMERICAN CHEMICAL SOCIETY
pubs.acs.org/JACS
Article

Dynamic Stability of Copper Single-Atom Catalysts under Working Conditions

Xiaowan Bai,[‖] Xunhua Zhao,[‖] Yehui Zhang, Chongyi Ling, Yipeng Zhou, Jinlan Wang,* and Yuanyue Liu*

Cite This: J. Am. Chem. Soc. 2022, 144, 17140−17148

ABSTRACT: The long-term stability of single-atom catalysts is a major factor affecting their large-scale commercial application. How to evaluate the dynamic stability of single-atom catalysts under working conditions is still lacking. Here, taking a single copper atom embedded in N-doped graphene as an example, the "constant-potential hybrid-solvation dynamic model" is used to evaluate the reversible transformation between copper single atoms and clusters under realistic reaction conditions. It is revealed that the adsorption of H is a vital driving force for the leaching of the Cu single atom from the catalyst surface. The more negative the electrode potential, the stronger the adsorption of H. As a result, the competitive hydrogen evolution reaction is inhibited, and Cu−N bonds are weakened, resulting in some Cu atoms being tethered on the catalyst surface and some being dissolved in the aqueous solution. The collision of the Cu atoms in the two states forms a transient Cu cluster structure as a true catalytic active site to promote CO_2 reduction to ethanol. As the applied potential is released or switched to a positive value, hydroxyl radicals ($OH^•$) play a dominant role in the oxidation process of the Cu cluster, and then Cu returns to the initial atomic dispersion state by redeposition, completing the reconstruction cycle of the copper catalyst. Our work provides a fundamental understanding of the dynamic stability of Cu single-atom catalysts under working conditions at the atomic level and calls for a reassessment of the stability of currently reported single-atom catalysts considering realistic reaction conditions.

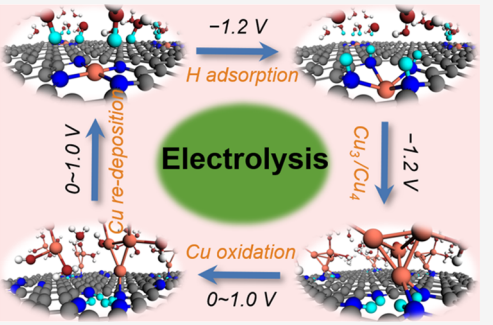

1. INTRODUCTION

As a new frontier catalytic material, supported single-atom catalysts (SACs) have attracted extensive attention in the recent decade since the concept of "single-atom catalysis" was first introduced by Zhang et al.[1] With the high atom utilization and remarkable catalytic activity, SACs exhibit great potential for applications for electrochemical energy conversion and storage processes, such as hydrogen evolution reaction (HER),[2] oxygen evolution reaction (OER),[3] carbon dioxide reduction (CO_2RR),[4,5] nitrogen reduction reaction (NRR),[6,7] oxygen reduction reaction (ORR),[8−10] etc. Despite numerous studies focusing on the design, synthesis, and application of SACs, their commercialization is still limited due to the pursuit of better activity and selectivity at the expense of stability, which is a more critical factor hindering large-scale applications.[11−13]

The instability of SACs is attributed to the high surface energy of metal single atoms prompting them to aggregate into more stable nanoparticles during conventional preparations,[14] such as the coexistence of Pt single atoms and nanoparticles, which often occurs in conventional substrates of Al_2O_3, SiO_2, and TiO_2.[15] Furthermore, SACs can undergo structural transformations into clusters under working conditions.[16] For instance, Frédéric et al. found that FeN_4C_{12} and FeN_4C_{10} moieties possess different stabilities with increasing operation time. The number of active sites for the former is reduced due to the formation of ferric oxides, resulting in the deactivation of the catalyst, while the number of catalytic active sites for the latter remains unchanged.[17] In addition, a more interesting structural transformation occurred on Cu SACs during CO_2 reduction. Fontecave et al.[18,19] reported that single-atom Cu^{2+} dispersed in the N-doped carbon material, under a certain range of negative electrode potential, could be transformed into Cu^0 small clusters. In turn, it can be restored to Cu^{2+} in the initial atomic dispersion state after releasing the applied potential or switching to a positive potential. Similar dynamic behavior was also observed by Xu et al.[20] It is even clearer that copper-based metal−organic frameworks with well-defined structures showed reversible dynamic reconstruction during working conditions. These transformation behaviors not only do not deactivate the catalysts but also act as true catalytic

Received: July 8, 2022
Published: September 12, 2022

https://doi.org/10.1021/jacs.2c07178
J. Am. Chem. Soc. 2022, 144, 17140−17148

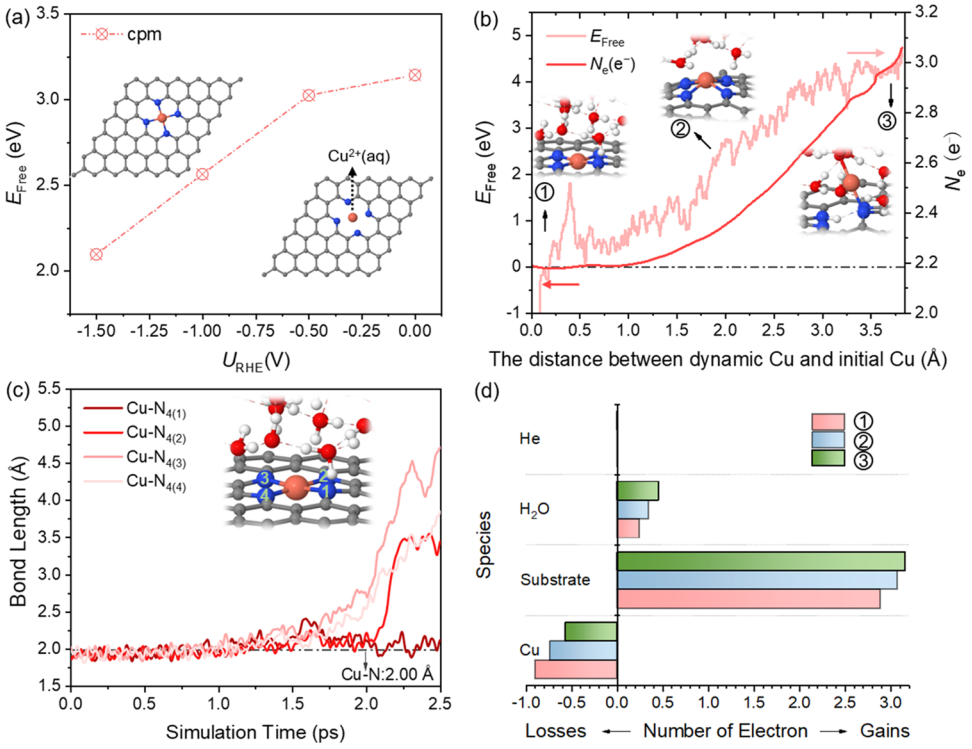

Figure 1. Thermodynamic and kinetic evaluation of the Cu SA leaching process from the double-vacancy (DV) defect site in N-doped graphene. (a) The free energy (ΔG) of Cu^{2+}(aq) formation during Cu SA leaching at different potentials. (b) Free energy profile and net electron evolution during the Cu SA leaching process under $U_{RHE} = -1.2$ V. The positive net number of electrons (N_e) represents gain, while the negative represents loss. (c) Dynamic evolution of the bond length of Cu−$N_{4(x)}$ (x = 1, 2, 3, and 4) during the Cu SA leaching process. The referenced bond length of Cu−N in a series of copper(II) Schiff base complexes is shown with a black dotted line.[37] (d) Bader charge analysis of the representative snapshot structures in (b), including Cu SA, substrate, water, and He. C: gray; N: blue; Cu: orange; O: red; H: white; He: green.

active sites, facilitating the efficient reduction of CO_2 to ethanol or methane.[21] However, the current evaluation of the stability of SACs is still mainly focused on thermodynamic "static" calculations, including formation energy,[22] cohesive energy,[23] binding energy,[2] diffusion barrier,[24] etc. Although molecular dynamics simulations can also be used to verify the stability of SACs, the most relevant studies do not consider the effects of kinetics, pH, working potential, and concentration of reactants or key intermediates on the structural stability in complex and realistic catalytic reactions.[25−27] Therefore, exploring the "dynamic" evolution of the structural and electrical properties of SACs under working conditions is a great challenge and is essential.

Herein, we construct a solid−liquid interface, namely, copper single-atom nitrogen-doped graphene (Cu−N_4−C) with explicit water layers, to study the dynamic stability of the Cu single-atom catalyst under working conditions using our recently developed constant-potential hybrid-solvation dynamical model (CP-HS-DM).[28] The calculation results demonstrate that the more negative the electrode potential, the stronger the adsorption of H at the N site, thus inhibiting the production of H_2, which is consistent with the experimental result.[18] Moreover, it is found that the adsorption of H is a vital driving force for the leaching of the Cu single atom (SA) from the catalyst surface during electrolysis, which can reduce the kinetic barrier to Cu SA leaching compared to the absence of H adsorption. After a portion of Cu atoms leach from the surface, they form transient steady-state Cu small cluster structures with adjacent and tethered Cu atoms, thus facilitating the reduction of CO_2 to ethanol. When the reaction is over, or the applied potential is adjusted to a positive value, the oxidation of Cu is greatly accelerated by $OH^{\bullet}$ and then redeposited, and finally, the Cu clusters are restored to the initial atomically dispersed state, completing the reconstruction cycle of the copper catalyst. Our work provides a new fundamental understanding of the dynamic stability of SACs under working conditions.

2. COMPUTATION METHODS

Structure optimization and ab initio molecular dynamics (AIMD) were carried out using density functional theory (DFT) as implemented in the Vienna ab initio Simulation Package (VASP 5.4.4).[29,30] The electronic exchange and correlation interactions were described by the Perdew−Burke−Ernzerhof (PBE) functional within the generalized gradient approximation (GGA).[31,32] The projector augmented wave (PAW) method[33] was applied to account for the core−valence interactions and the cutoff energy of the plane-wave basis was set to be 400 eV in the relaxation, while 300 eV was used in the AIMD simulations at 300 K. The convergence criteria of energy and force are 0.01 eV/Å and 10^{-5} eV for relaxing structures, respectively. The PBE-D3 method[34] was employed to correct van der Waals interaction of water−water and water−substrate. A 3 × 3 × 1 gamma-centered k-mesh was used in the relaxation, while the gamma point of the Brillouin zone with no consideration of symmetry was adopted in the AIMD simulations. The time step in AIMD was set to be 0.5 fs. The dynamic stability of the catalyst structures under operating potential was evaluated by CP-HS-DM.[28] The net electronic charges were balanced by the ionic charges in the implicit solution, and thus, the total system remains charge neutral. The compensation charges were added as point charges, following the Poisson−Boltzmann distribution. This has been implemented to

https://doi.org/10.1021/jacs.2c07178
J. Am. Chem. Soc. 2022, 144, 17140−17148

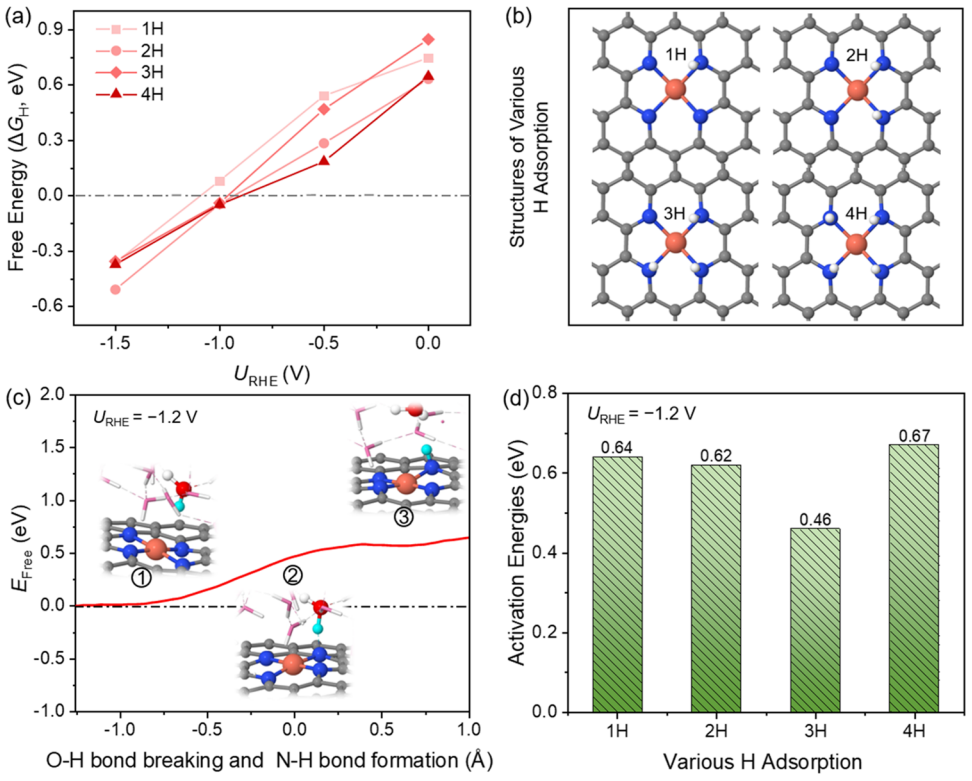

Figure 2. (a) Free energy (ΔG_H) of the 1st, 2nd, 3rd, and 4th H adsorption under different potentials. (b) The structures of *x*H adsorption at the N sites. (c) Free energy profile during the hydrolysis of the first H_2O to form H* and OH^-. The cyan sphere represents H^+ that will be electrolyzed from the first H_2O. (d) The activation energies for each (c) process with the number of H adsorption.

VASP as VASPsol.[35] More details can be found in the Supporting Information.

3. RESULTS AND DISCUSSION

The prerequisite of Cu SA leaching from the surface to form a small Cu cluster during CO_2RR is that the Cu−N bond becomes weak and easy to break. Therefore, the possibility of Cu SA leaching is evaluated in thermodynamics and kinetics separately. The free energies of the leaching of Cu single atoms anchored on the substrate to form solvent cations $Cu^{2+}(aq)$ are calculated for determining the thermodynamic stability of the Cu single-atom catalyst. Similar to the computational hydrogen electrode method,[36] the free energy of the Cu ion $G(Cu^{2+}(aq))$ is obtained from the experimental standard hydrogen electrode U_0 and the calculated free energy of the bulk metal $G(Cu(s))$ as follows

$$Cu^{2+}(aq) + 2e^- \leftrightarrow Cu(s) \quad (1)$$

$$G(Cu^{2+}(aq)) = G(Cu(s)) - 2\mu_e \quad (2)$$

$$\mu_e = \mu_{SHE} - |e|U_0 \quad (3)$$

where μ_e is the electron energy, μ_{SHE} is benchmarked to be −4.6 eV for VASPsol,[35] and U_0 = 0.34 V.

The leaching process is as follows

$$Cu - N_4 - C \leftrightarrow N_4 - C + Cu^{2+}(aq) + 2e^- \quad (4)$$

Thus, the corresponding reaction free energies at a constant potential U can be calculated as

$$\Delta G = G(N_4 - C^{*Q2}) + G(Cu^{2+}(aq)) - G(Cu - N_4 - C^{*Q1}) + 2|e|U + (Q2 + 2 - Q1)\mu_e$$

where $Q1$ and $Q2$ are the net charges on the Cu−N_4−C and N_4−C surfaces, respectively. Note that to balance the charge, the number of electrons involved changes to $Q2 + 2 - Q1$.

Figure 1a shows the free energies of Cu SA leaching from the surface to form $Cu^{2+}(aq)$ at different electrode potentials from 0 to −1.5 V vs reversible hydrogen electrode (RHE). Although the free energy decreases to 2.09 eV at −1.5 V vs RHE, it is still thermodynamically difficult to leach from the surface. We further evaluate the kinetic possibility of Cu leaching from the surface by CP-HS-DM. Here, the referenced electrode potential is −1.2 V vs RHE, since the highest faradaic yield of ethanol can be obtained at this corresponding potential.[18] A solid−liquid interface model is constructed in Figure S1. In this structure, an inert He atom is introduced as a rivet and fixed at a distance of 18.28 Å directly above the Cu atom, using it to calculate the kinetic activation energy of Cu SA leaching from the N_4−C site. The chosen reaction coordinate in the "slow-growth" approach is that the distance between Cu and He atoms is shortened (see Figure S3a). For more visualization, the horizontal coordinates in Figure 1b are converted to the distance between dynamic Cu and initial Cu. The free energy continues to increase as Cu moves away from the surface, reaching up to 4.74 eV at the end of the reaction. This result indicates that the four Cu−N bonds are difficult to break, and Cu SA cannot be leached from the surface at room temperature. The dynamic evolution of the bond length of Cu−N with the Cu SA leaching process is tracked in Figure 1c.

https://doi.org/10.1021/jacs.2c07178
J. Am. Chem. Soc. 2022, 144, 17140−17148

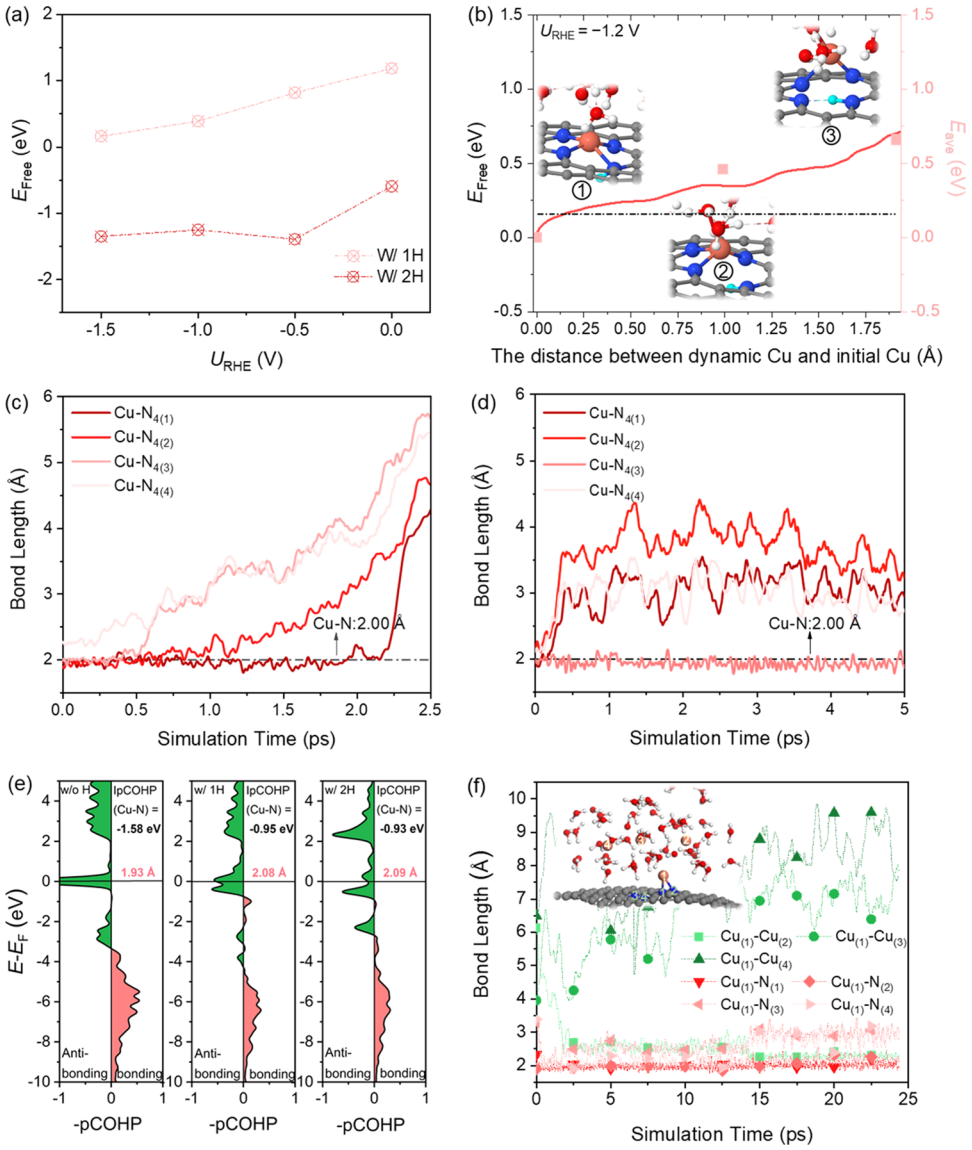

Figure 3. (a) Free energy (ΔG) of the Cu SA leaching process for the formation of Cu^{2+}(aq) with xH (x = 1, 2) adsorption under different potentials. (b) Free energy profile and average energy during the Cu SA leaching process under one H atom adsorption at an N atom at U_{RHE} = −1.2 V. (c) Dynamic evolution of the bond length of Cu−$N_{4(x)}$ (x = 1, 2, 3, and 4) under one H atom adsorption during the Cu SA leaching process. (d) With adsorption of two H atoms, simulating by a constant-potential AIMD of 5 ps. The referenced bond length of Cu−N in a series of copper(II) Schiff base complexes is shown with the black dotted line.[37] (e) Projected crystal orbital Hamilton population (pCOHP) between the central copper atom and the nitrogen atom as H adsorption increases at −1.2 V vs RHE. Corresponding IpCOHP values (black) and Cu−N bond lengths (red) are shown in the figures. The more negative the IpCOHP value, the more stable the bond under consideration. (f) Dynamic evolution of the bond length in the collision process of one tethered Cu and three free Cu atoms during an AIMD simulation of 24 ps at U_{RHE} = −1.2 V.

Note that one water molecule close to the $N_{(3)}$ atom undergoes hydrolysis when the Cu−$N_{(3)}$ bond is broken and the corresponding configuration at the end of the reaction is that the Cu atom is only coordinated with one N atom and one −OH group, which is in accordance with the experimental EXAFS spectra data.[18] Figure 1b shows the change in the number of electrons with the evolution of the structure. Compared with the initial structure, the net charge number of the final structure increases to about 0.7 e^- due to the formation of OH^-. Bader charge analysis of the representative snapshots in Figure 1b is shown in Figure 1d, including Cu SA, substrate, water, and He atom. Obviously, the He atom does not gain or lose electrons in the whole process, which has a negligible effect on the charge of the whole system. Interestingly, the number of electrons lost by Cu decreases from 0.9 e^- in the initial structure to 0.56 e^- in the final structure, indicating that Cu SA leaching from the surface tends to be metallic Cu, which is in agreement with the experimental observation that the Cu oxidation state changes from +2 to 0.[18] Therefore, both thermodynamic and kinetic results indicate that it is almost impossible for the Cu SA to leach directly from the surface.

However, the existence of a structural transformation between atomically dispersed Cu^{+2} and metallic Cu^0 small clusters through X-ray absorption spectroscopy (XAS) characterization in operando CO_2 electrolysis conditions has indeed been confirmed.[18,20,21] What is the driving force for the leaching of Cu SA from the N_4−C site with the strong

https://doi.org/10.1021/jacs.2c07178
J. Am. Chem. Soc. 2022, 144, 17140−17148

chelating capacity to form Cu clusters? Does H_2 as a competitive product for CO_2 reduction affect structural transformation? To solve these confusions, the H adsorption behavior under the CO_2 reduction potential is explored. Figure 2a,b shows free energies as a function of the applied electrode potential and configurations of xH adsorption (x = 1, 2, 3, and 4), respectively. As the electrode potential changes from zero to negative, the corresponding free energies of H adsorption convert from positive to a negative value, indicating that the adsorption of H at the N sites is thermodynamically converted from unfavorable to favorable. This transformation is ascribed to the fact that the potential becomes more negative, resulting in more electron accumulation on the catalyst surface, thus promoting the adsorption of H^+ (see Table S1). Note that the calculations of free energy based on the conventional first-principles method show that the H adsorption on $N_{(x)}$ (x = 1, 2, 3, and 4) sites is thermodynamically unfavorable, as shown in Figure S6. These results adequately demonstrate that it is critical to consider the surface charge effect in electrochemical reactions.[38,39] More interestingly, our calculation gives a ΔG_H value close to zero at U_{RHE} = −1.0 V, which explains why the faradaic yield of H_2 as the major reaction product is the highest at −1.0 V in the experiment.[18] At U_{RHE} = −1.2 V, the hydrogen evolution reaction (HER) is effectively suppressed due to the significant enhancement of H adsorption. We speculate that the adsorption of H may be an important factor affecting Cu desorption at a negative potential (which will be discussed later). The source of H is further discussed. There is only one possibility, that is, hydrolysis. Therefore, the kinetic barrier for the hydrolysis of the first H_2O to form H* and OH^- is calculated (see Figures 2c and S3b). The criterion for the end of this reaction is that the difference between the N−H and O−H bond lengths is 1.00 Å in Figure S7a, and the energy barrier is 0.64 eV at −1.2 V, indicating that this reaction easily occurs at room temperature. Note that the difference in the number of electrons before and after the reaction is about 0.8 e^-, which confirms the production of OH^- (see Figure S7b). To have an idea of how much the randomness of the AIMD can impact the results, incremental speeds of 0.0004 and 0.0012 are considered for the hydrolysis of the first H_2O, as shown in Figure S8. The calculations show that the energy barrier fluctuates within ±0.05 eV, indicating that the accuracy of the calculations employed in these AIMD simulations is acceptable. Although the energy barrier for H adsorption is relatively low, the energy of the final state is higher than that of the initial state. One may wonder if removing the constraint can automatically reverse the process to the initial state, so an unconstrained AIMD simulation of 2 ps is performed. The calculated results show that it takes 1.37 ps for the adsorbed H to return to the solution (Figure S9a). H returns because there is a OH^- in the aqueous solution. Under real electrochemical conditions, OH^- may diffuse into the bulk of the solution and reduces the free energy, resulting in adsorbed H not returning to the solution.[40,41] Since the structure of the catalyst contains four N atoms, it can provide four active sites for H adsorption, and the activation energies of the remaining three N sites occupied by H also are calculated, which are 0.62, 0.46, and 0.67 eV (Figures 2d and S10). The average barrier for the hydrolysis of H_2O to form *H and OH^- is about 0.60 eV. Therefore, we verify from both thermodynamics and kinetics that H from the H_2O molecule can be adsorbed to the N sites at U_{RHE} = −1.2 V.

Next, we try to answer the remaining question above: how does the adsorption of H affect the transformation of the catalyst structure during CO_2 reduction? The free energy (ΔG) of Cu^{2+}(aq) formation during Cu SA leaching under 1H and 2H adsorption is calculated and shown in Figure 3a. With the adsorption of H, the binding strength between Cu SA and the substrate is weakened, leading to a thermodynamically unfavorable to favorable leaching process of Cu SA. Back to the dynamics, the kinetic barrier for the Cu SA leaching process from the $Cu-N_4-C$ substrate is re-evaluated, where one N site is adsorbed by one H. An activation energy of 0.70 eV is taken from the energy of the 2500th step (1.25 ps) in Figure 3b, corresponding to the coordination of Cu with one N atom and one H_2O molecule. This is consistent with the experimental observation that Cu coordinates with light atoms (C, N, O) during CO_2RR. We further perform augmented sampling of the snapshot structures in Figure 3b and an AIMD simulation of 2.5 ps for each structure in a fixed collective variable to obtain a kinetic energy barrier of 0.66 eV (see Figure S11), which is consistent with the slow-growth results. In addition, an unconstrained AIMD simulation of 1.5 ps is performed, and it is observed that the Cu single atom is not returned to the initial state, indicating that the final state is a relatively stable state (Figure S9b). Compared with a pure $Cu-N_4-C$ surface (4.74 eV), the adsorption of H significantly promotes the leaching of Cu SA. As shown in Figure 3c, when the constrained MD reaches 2.25 ps, the Cu atom is completely detached from the surface, dissolved in an aqueous solution and attached to two H_2O molecules. Unexpectedly, Figure 3d shows the dynamic evolution of the bond length of $Cu-N_{4(x)}$ (x = 1, 2, 3, and 4), indicating that the Cu SA spontaneously leaches from the surface in a short time (∼300 fs) under the condition of 2H coadsorption. The obtained final configurations are composed of one Cu−N bond and at least one Cu−O bond. The complete leaching of Cu is further evaluated by the slow-growth method at a time of 2.5 ps, as shown in Figure S12. An energy barrier of 0.84 eV is obtained, indicating that this reaction can occur in mild conditions, but is slightly higher by 0.14 eV than the incomplete leaching of Cu (0.70 eV). Thus, at a dynamic electrochemical interface, Cu should exist in two transient states, i.e., incomplete leaching combined with one N atom and complete leaching dissolved in water. As the applied potential becomes more negative, H adsorption is easier, leading to a more indirect promotion of Cu leaching (see Figure S13). The projected crystal orbital Hamilton population (pCOHP)[42,43] is used to analyze the bond strength between the central copper atom and the nitrogen atom as H adsorption increases. As shown in Figure 3e, the contribution of the antibonding orbital population below the Fermi level increases with the increase in the number of H adsorbed, which weakens the strength of the Cu−N bond. In addition, the integrated pCOHP (IpCOHP) can quantitatively provide bond strength information.[44] The IpCOHP values of one Cu−N bond in the $Cu-N_4-C$ are given in Figure 3e, corresponding to −1.58 for the bare surface, −0.95 for 1H, and −0.93 eV for 2H. Obviously, as the number of H adsorbed increases, the absolute value of IpCOHP becomes smaller, indicating that the Cu−N bond becomes weaker, which leads to the transition from difficult to spontaneous leaching of the Cu single atom. Therefore, the adsorption of H is a vital driving force that leads to the leaching of the Cu SA from the catalyst surface. The dynamic evolution of the bond length of $Cu-N_{4(x)}$ (x = 1, 2, 3, and 4)

https://doi.org/10.1021/jacs.2c07178
J. Am. Chem. Soc. 2022, 144, 17140−17148

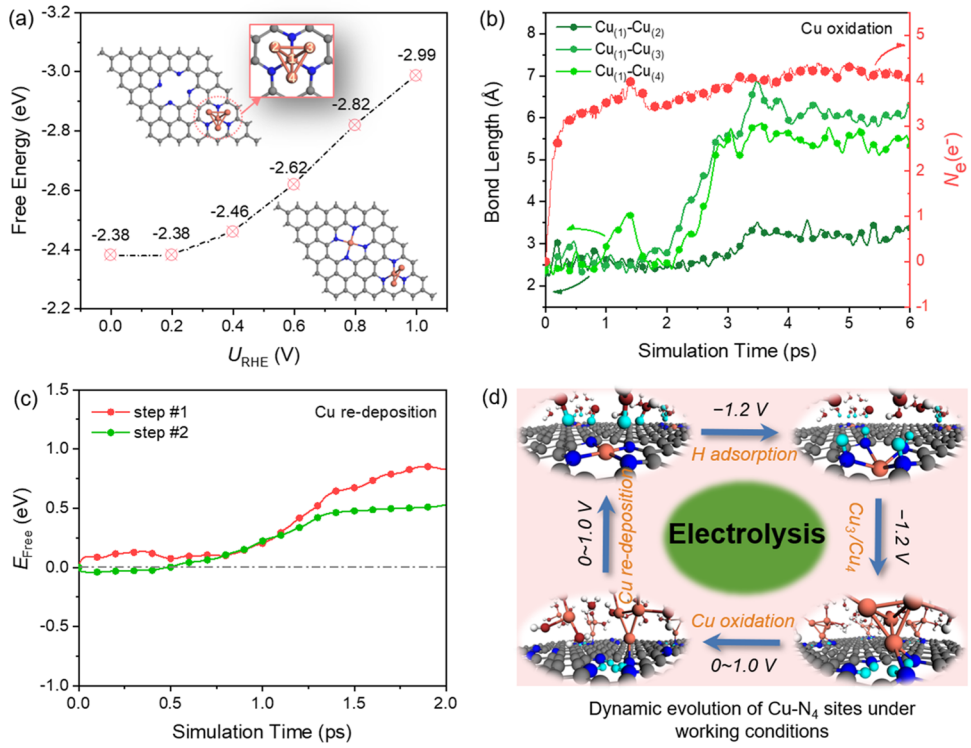

Figure 4. (a) Free energy of leaching a Cu atom from the Cu_4 cluster anchored on the substrate. (b) Dynamic evolution of the bond length of Cu−Cu and the net electron at the Cu_4 cluster with two OH• during an AIMD simulation of 6 ps at U_{RHE} = 1.0 V. (c) Free energy profiles of Cu redeposition during 2.0 ps slow-growth simulation at U_{RHE} = 1.0 V. (d) Summary illustration of the mechanism of the dynamic reversible transformation of the Cu single-atom cluster catalytic structure under working conditions.

and pCOHP analysis under the conditions of 3H and 4H coadsorption is shown in Figures S14 and S15, respectively. The effect on the Cu leaching behavior is consistent with the results of the two H adsorption. In addition to the adsorption of H on N sites, the adsorbates also have an important effect on the Cu single atom itself. Five intermediates (H, CO, CO_2, H_2O, and OH) are considered for adsorption on the Cu single atom (Figure S16). The strength of the weakening of the Cu−N bond is CO > H(Cu) > H(N) > OH > CO_2 > H_2O. However, due to the lack of saturation of N, the adsorption of CO and H on Cu single atoms (0.79 and 2.03 eV, respectively) is unfavorable compared to H on N (0.28 eV) in the leaching of Cu. Therefore, the adsorption of H on the N site is more likely to promote the leaching of the Cu single atom from the catalytic surface.

As mentioned above, some Cu atoms remain connected to the N atoms and are tethered to the catalyst surface, while some Cu atoms dissolve in the aqueous solution. Under a dynamic environment, the collision of the Cu atoms in the two states forms a transient $Cu_{3/4}$ cluster structure as the true catalytic active center. We further simulate the aggregation process of Cu atoms under working conditions. It is observed in Figure 3f that the two Cu atoms aggregate is less than 2.5 ps during AIMD and the $Cu_{(1)}$ atom remains bound to $N_{(1)}$ and $N_{(2)}$. At 15 ps, the bond length of $Cu_{(1)}$−$Cu_{(2)}$ was further shortened to 2.26 Å, and the bond lengths of $Cu_{(1)}$−$N_{(3)}$ and $Cu_{(1)}$−$N_{(4)}$ were stretched to 3.09 and 3.03 Å, respectively. Due to such a high computational cost, the dynamic simulation calculations on the formation of $Cu_{3/4}$ small clusters had to be stopped, but we believe that the $Cu_{3/4}$ cluster will be observed in long simulations in a dynamic solid−liquid interface environment. Once more and more Cu small clusters are formed, they can accelerate the CO_2 reduction to ethanol. Our previous study has proved that the Cu_4 cluster supported on *g*-C_3N_4 can promote the reduction of CO_2 to ethanol.[45] To date, the restructuring dynamic process of Cu single atoms forming Cu clusters has been clearly understood during the CO_2 reduction reaction.

After the CO_2 reduction reaction is over, the electrode potential is switched off to stop the electrocatalytic reaction or to +1.0 V vs RHE. At this time, the Cu small clusters (Cu^0) can be restored to atomically dispersed copper (Cu^{2+}).[38,39,46] Compared to the leaching process of Cu SA, the return of the Cu atom is more complex and challenging in the simulation. The formation of Cu−N_4 sites is accompanied by oxidation of the metallic copper under the positive electrode potential, resulting in the oxidation state of Cu increasing to +2. Here, simple Cu_4 and Cu SA−Cu_3 models are used to describe the electrochemical deposition process in thermodynamics (see Figure S17). The free energy of the Cu SA−Cu_3 formation becomes more negative as the potential increases, which means that the production of Cu SA−Cu_3 is more favorable, as shown in Figure 4a. Recently, an experimental study has confirmed that the occurrence of fast oxygen exchange between HCO_3^- and H_2O facilitates the formation of the highly oxidative hydroxyl radicals (OH•), which leads to the promotion of the fast reoxidation of Cu.[47] Therefore, we consider the introduction of two OH• radicals in the system to assess the reoxidation process of the Cu_4 cluster at +1.0 V vs RHE. The two configurations, including a Cu_4 cluster combined with two OH• radicals ($Cu_4(OH•)_2$) and a Cu_3 cluster with an escaped Cu atom bonded to two OH• radicals (Cu_3 + $Cu(OH•)_2$), are constructed and performed for AIMD simulations of 6 and 2.5 ps, respectively. Figures 4b and S18 show that two OH•

https://doi.org/10.1021/jacs.2c07178
J. Am. Chem. Soc. 2022, 144, 17140−17148

radicals oxidize the first coordination shell of Cu−Cu after 2 and 0.5 ps, respectively. After this, the $Cu_{(1)}$ atom bonded to the catalyst substrate is farther and farther away from the other three or two Cu atoms. For Cu_3 + $Cu(OH^{\bullet})_2$, the $OH^{\bullet}$ radical runs completely onto the Cu_3 cluster to carry out further oxidation after 0.5 ps, while the escaped Cu is coordinated with the three H_2O molecules ($Cu_3(OH^{\bullet})_2$ + $Cu(H_2O)_3$). Therefore, the presence of $OH^{\bullet}$ radicals plays a dominant role in the fast reoxidation of Cu compared to pure aqueous solutions (Figure S19). It is noted that the net charge of the system is in relative equilibrium during the oxidation process, and almost no additional electrons are transferred to the electrodes, indicating that the Cu cluster is oxidized to $Cu^{\delta+}$ by $OH^{\bullet}$ radicals. After the formation of $Cu(H_2O)_3$, the Cu redeposition process occurs when $Cu(H_2O)_3$ diffuses to the adjacency of the N_4−C site, i.e., Cu migrates from an aqueous solution to be coordinated with a N atom as step #1, overcoming a kinetic energy barrier of 0.85 eV (Figure 4c). The Cu−$O_{(1,2,3)}$ and Cu−N bonds (Figure S20) are 2.12, 2.15, 2.20, and 2.06 Å, respectively. Furthermore, similar to the Cu leaching process, to avoid the complexity of multiple reaction paths, the He atom is again introduced directly below the Cu atom (the *Z*-direction of the He atom is fixed). The reaction path of the Cu back to the N_4−C vacancy process is simplified to a shortening of the Cu−He bond as step #2, overcoming an energy barrier of 0.50 eV. During this reaction, three H_2O molecules return to the aqueous solution with an average bond length of 1.94 Å for Cu−N bonds (Figure S21), consistent with the experimental characterization for the initial Cu−N bond length (1.95 Å).[18] That is, once the Cu atom is coordinated to one N, the Cu atom quickly returns to its initially dispersed state. Therefore, the synergistic effect between highly oxidative $OH^{\bullet}$ and the strong chelating ability of the N_4−C site under a positive potential promotes the return of the Cu cluster to the Cu SA state, completing the cycle of restructuring behavior. Figure 4d shows a dynamic and reversible transformation mechanism between the Cu SA to the $Cu_{3/4}$ small clusters during electrolysis. It is mainly divided into two processes, that is, the escape and return of the Cu SA. The adsorption of H under a negative potential promotes the conversion of the Cu SA to Cu clusters, thereby optimizing the performance of the catalyst and enhancing the selectivity of ethanol. When the electrode potential is switched off or to a positive value, Cu SA returns to the atomic dispersion through oxidation and redeposition processes. To better understand the specificity of the structural transformation of Cu−N_4−C during CO_2 reduction, we also consider the free energy of one H adsorption on a Cu single atom coordinated with O_4−C and Fe, Co, and Ni coordinated with N_4−C at U = −1.2 V. The calculated results indicate that the Cu−N bond is the weakest among all of the M−N bonds, which is consistent with the metal leaching phenomenon reported in experiments for Cu only during CO_2RR.[18−21] More details can be found in the Supporting Information (Figures S22 and S23).

4. CONCLUSIONS

In summary, we have systematically investigated the dynamic stability of the Cu single-atom catalyst under working conditions, namely, the reversible transformation between Cu SA and $Cu_{3/4}$ clusters, using the "constant-potential hybrid-solvation dynamic model". We reveal that the adsorption of H, depending on the potential, is a crucial driving force for the conversion of Cu single atoms into Cu clusters, while the reversion of Cu clusters to the atomic dispersion state is dominated by oxidation reactions, and $OH^{\bullet}$ plays a crucial role in this process. These results are impossible to be identified using the previous charge-neutral DFT calculations. As a result, considering the effect of surface charge and explicit water solvent is an important means to understand the dynamic stability of SACs under working conditions. We expect a systematic exploration of the stability of SACs in real electrochemical reactions in the future. In addition to SACs, the studies on the oxidation state and surface reconstruction of copper catalysts under CO_2 reduction conditions have been recently reported experimentally.[48−50] Although these studies reveal that the applied electrode potential is the dominant factor in the surface reconstruction of copper catalysts during CO_2 reduction, the mechanism for the reconstruction of the catalysts is unclear. Therefore, an in-depth understanding of the dynamic stability of catalysts, whether SACs or bulk materials, can provide not only a fundamental understanding of the evolution of structural and electrical properties under operating conditions but also new ideas for the design and development of catalysts with better performance.

■ ASSOCIATED CONTENT

Supporting Information

The Supporting Information is available free of charge at https://pubs.acs.org/doi/10.1021/jacs.2c07178.

Construction of models and computation details; raw data from AIMD and the constrained MD simulations; dynamic evolution of the bond length and surface charge; free energies and activation energies for H adsorption; and pCOHP comparison for *x*H adsorption at N sites (where x = 0, 1, 2, 3, and 4) (PDF)

■ AUTHOR INFORMATION

Corresponding Authors

Jinlan Wang − *School of Physics, Southeast University, Nanjing 211189, China;* orcid.org/0000-0002-4529-874X; Email: jlwang@seu.edu.cn

Yuanyue Liu − *Texas Materials Institute and Department of Mechanical Engineering, The University of Texas at Austin, Austin, Texas 78712, United States;* orcid.org/0000-0002-5880-8649; Email: yuanyue.liu@austin.utexas.edu

Authors

Xiaowan Bai − *School of Physics, Southeast University, Nanjing 211189, China; Texas Materials Institute and Department of Mechanical Engineering, The University of Texas at Austin, Austin, Texas 78712, United States*

Xunhua Zhao − *Texas Materials Institute and Department of Mechanical Engineering, The University of Texas at Austin, Austin, Texas 78712, United States; Macao Institute of Materials Science and Engineering (MIMSE) and Zhuhai MUST Science and Technology Research Institute, Faculty of Innovation Engineering, Macau University of Science and Technology, Macau 999078, China*

Yehui Zhang − *School of Physics, Southeast University, Nanjing 211189, China*

Chongyi Ling − *School of Physics, Southeast University, Nanjing 211189, China;* orcid.org/0000-0002-4126-9036

Yipeng Zhou − *School of Physics, Southeast University, Nanjing 211189, China*

Complete contact information is available at:
https://pubs.acs.org/10.1021/jacs.2c07178

Author Contributions

[‖]X.B. and X.Z. contributed to the work equally.

Notes

The authors declare no competing financial interest.

■ ACKNOWLEDGMENTS

J.W. acknowledges the support by the National Natural Science Foundation of China (Grant Nos. 22033002 and 22173018) and the National Key Research and Development Program of China (2021YFA1500700). The authors are thankful for the computational resources from the Big Data Center of Southeast University and the National Supercomputing Center of Tianjin. Y.L. acknowledges the support by NSF (Grant Nos. 1900039, 2029442), ACS PRF (60934-DNI6), and the Welch Foundation (Grant No. F-1959-20210327). The calculations used computational resources at XSEDE, TACC, Argonne National Lab, and Brookhaven National Lab. C.L. acknowledges Basic Research Program of Jiangsu Province (BK20220800).

■ REFERENCES

(1) Qiao, B.; Wang, A.; Yang, X.; Allard, L. F.; Jiang, Z.; Cui, Y.; Liu, J.; Li, J.; Zhang, T. Single-atom catalysis of CO oxidation using Pt_1/FeO_x. *Nat. Chem.* **2011**, *3*, 634−641.

(2) Zhuo, H.-Y.; Zhang, X.; Liang, J.-X.; Yu, Q.; Xiao, H.; Li, J. Theoretical Understandings of Graphene-based Metal Single-Atom Catalysts: Stability and Catalytic Performance. *Chem. Rev.* **2020**, *120*, 12315−12341.

(3) Ling, C.; Shi, L.; Ouyang, Y.; Zeng, X. C.; Wang, J. Nanosheet Supported Single-Metal Atom Bifunctional Catalyst for Overall Water Splitting. *Nano Lett.* **2017**, *17*, 5133−5139.

(4) Zhang, J.; Cai, W.; Hu, F. X.; Yang, H.; Liu, B. Recent advances in single atom catalysts for the electrochemical carbon dioxide reduction reaction. *Chem. Sci.* **2021**, *12*, 6800−6819.

(5) Guo, W.; Tan, X.; Bi, J.; Xu, L.; Yang, D.; Chen, C.; Zhu, Q.; Ma, J.; Tayal, A.; Ma, J.; et al. Atomic Indium Catalysts for Switching CO_2 Electroreduction Products from Formate to CO. *J. Am. Chem. Soc.* **2021**, *143*, 6877−6885.

(6) Ling, C.; Bai, X.; Ouyang, Y.; Du, A.; Wang, J. Single Molybdenum Atom Anchored on N-Doped Carbon as a Promising Electrocatalyst for Nitrogen Reduction into Ammonia at Ambient Conditions. *J. Phys. Chem. C* **2018**, *122*, 16842−16847.

(7) Ding, S.; Hülsey, M. J.; Pérez-Ramírez, J.; Yan, N. Transforming Energy with Single-Atom Catalysts. *Joule* **2019**, *3*, 2897−2929.

(8) Wang, Y.; Tang, Y.-J.; Zhou, K. Self-Adjusting Activity Induced by Intrinsic Reaction Intermediate in Fe−N−C Single-Atom Catalysts. *J. Am. Chem. Soc.* **2019**, *141*, 14115−14119.

(9) Liu, K.; Fu, J.; Lin, Y.; Luo, T.; Ni, G.; Li, H.; Lin, Z.; Liu, M. Insights into the activity of single-atom Fe-N-C catalysts for oxygen reduction reaction. *Nat. Commun.* **2022**, *13*, No. 2075.

(10) Tang, C.; Chen, L.; Li, H.; Li, L.; Jiao, Y.; Zheng, Y.; Xu, H.; Davey, K.; Qiao, S.-Z. Tailoring Acidic Oxygen Reduction Selectivity on Single-Atom Catalysts via Modification of First and Second Coordination Spheres. *J. Am. Chem. Soc.* **2021**, *143*, 7819−7827.

(11) Yang, Y.; Lai, L.; Wei, L.; Chen, Y. Degradation: A critical challenge for M−N−C electrocatalysts. *J. Energy Chem.* **2021**, *63*, 667−674.

(12) Hu, H.; Wang, J.; Tao, P.; Song, C.; Shang, W.; Deng, T.; Wu, J. Stability of single-atom catalysts for electrocatalysis. *J. Mater. Chem. A* **2022**, *10*, 5835−5849.

(13) Zhao, X.; Levell, Z. H.; Yu, S.; Liu, Y. Atomistic Understanding of Two-dimensional Electrocatalysts from First Principles. *Chem. Rev.* **2022**, *122*, 10675−10709.

(14) Yang, X.-F.; Wang, A.; Qiao, B.; Li, J.; Liu, J.; Zhang, T. Single-Atom Catalysts: A New Frontier in Heterogeneous Catalysis. *Acc. Chem. Res.* **2013**, *46*, 1740−1748.

(15) Ding, K.; Gulec, A.; Johnson, A. M.; Schweitzer, N. M.; Stucky, G. D.; Marks, L. D.; Stair, P. C. Identification of active sites in CO oxidation and water-gas shift over supported Pt catalysts. *Science* **2015**, *350*, 189−192.

(16) Liu, L.; Meira, D. M.; Arenal, R.; Concepcion, P.; Puga, A. V.; Corma, A. Determination of the Evolution of Heterogeneous Single Metal Atoms and Nanoclusters under Reaction Conditions: Which Are the Working Catalytic Sites? *ACS Catal.* **2019**, *9*, 10626−10639.

(17) Li, J.; Sougrati, M. T.; Zitolo, A.; Ablett, J. M.; Oğuz, I. C.; Mineva, T.; Matanovic, I.; Atanassov, P.; Huang, Y.; Zenyuk, I.; et al. Identification of durable and non-durable FeNx sites in Fe−N−C materials for proton exchange membrane fuel cells. *Nat. Catal.* **2021**, *4*, 10−19.

(18) Karapinar, D.; Huan, N. T.; Ranjbar Sahraie, N.; Li, J.; Wakerley, D.; Touati, N.; Zanna, S.; Taverna, D.; Galvão Tizei, L. H.; Zitolo, A.; et al. Electroreduction of CO_2 on Single-Site Copper-Nitrogen-Doped Carbon Material: Selective Formation of Ethanol and Reversible Restructuration of the Metal Sites. *Angew. Chem., Int. Ed.* **2019**, *58*, 15098−15103.

(19) Creissen, C. E.; Fontecave, M. Keeping sight of copper in single-atom catalysts for electrochemical carbon dioxide reduction. *Nat. Commun.* **2022**, *13*, No. 2280.

(20) Xu, H.; Rebollar, D.; He, H.; Chong, L.; Liu, Y.; Liu, C.; Sun, C.-J.; Li, T.; Muntean, J. V.; Winans, R. E.; et al. Highly selective electrocatalytic CO_2 reduction to ethanol by metallic clusters dynamically formed from atomically dispersed copper. *Nat. Energy* **2020**, *5*, 623−632.

(21) Weng, Z.; Wu, Y.; Wang, M.; Jiang, J.; Yang, K.; Huo, S.; Wang, X.-F.; Ma, Q.; Brudvig, G. W.; Batista, V. S.; et al. Active sites of copper-complex catalytic materials for electrochemical carbon dioxide reduction. *Nat. Commun.* **2018**, *9*, No. 415.

(22) Guo, X.; Lin, S.; Gu, J.; Zhang, S.; Chen, Z.; Huang, S. Simultaneously Achieving High Activity and Selectivity toward Two-Electron O_2 Electroreduction: The Power of Single-Atom Catalysts. *ACS Catal.* **2019**, *9*, 11042−11054.

(23) Choi, C.; Back, S.; Kim, N.-Y.; Lim, J.; Kim, Y.-H.; Jung, Y. Suppression of Hydrogen Evolution Reaction in Electrochemical N_2 Reduction Using Single-Atom Catalysts: A Computational Guideline. *ACS Catal.* **2018**, *8*, 7517−7525.

(24) Xu, L.; Xie, M.; Yang, H.; Yu, P.; Ma, B.; Cheng, T.; Goddard, W. A. In-Silico Screening the Nitrogen Reduction Reaction on Single-Atom Electrocatalysts Anchored on MoS_2. *Top. Catal.* **2022**, *65*, 234−241.

(25) Cao, H.; Xia, G.-J.; Chen, J.-W.; Yan, H.-M.; Huang, Z.; Wang, Y.-G. Mechanistic Insight into the Oxygen Reduction Reaction on the $Mn-N_4/C$ Single-Atom Catalyst: The Role of the Solvent Environment. *J. Phys. Chem. C* **2020**, *124*, 7287−7294.

(26) Niu, H.; Zhang, Z.; Wang, X.; Wan, X.; Shao, C.; Guo, Y. Theoretical Insights into the Mechanism of Selective Nitrate-to-Ammonia Electroreduction on Single-Atom Catalysts. *Adv. Funct. Mater.* **2021**, *31*, No. 2008533.

(27) Zhang, W.; Fu, Q.; Luo, Q.; Sheng, L.; Yang, J. Understanding Single-Atom Catalysis in View of Theory. *JACS Au* **2021**, *1*, 2130−2145.

(28) Zhao, X.; Liu, Y. Origin of Selective Production of Hydrogen Peroxide by Electrochemical Oxygen Reduction. *J. Am. Chem. Soc.* **2021**, *143*, 9423−9428.

(29) Kresse, G.; Furthmuller, J. Efficiency of Ab-Initio Total Energy Calculations for Metals and Semiconductors Using a Plane-Wave Basis Set. *Comput. Mater. Sci.* **1996**, *6*, 15−50.

(30) Kresse, G.; Hafner, J. Ab initio molecular-dynamics for liquid-metals. *Phys. Rev. B* **1993**, *47*, 558−561.

(31) Perdew, J. P.; Chevary, J. A.; Vosko, S. H.; Jackson, K. A.; Pederson, M. R.; Singh, D. J.; Fiolhais, C. Atoms, Molecules, Solids, and Surfaces: Applications of the Generalized Gradient Approx-

imation for Exchange and Correlation. *Phys. Rev. B* **1992**, *46*, 6671−6687.
(32) Ernzerhof, M.; Perdew, J. P. Generalized gradient approximation to the angle- and system-averaged exchange hole. *J. Chem. Phys.* **1998**, *109*, 3313−3320.
(33) Blöchl, P. E. Projector augmented-wave method. *Phys. Rev. B* **1994**, *50*, 17953−17979.
(34) Grimme, S.; Antony, J.; Ehrlich, S.; Krieg, H. A consistent and accurate ab initio parametrization of density functional dispersion correction (DFT-D) for the 94 elements H-Pu. *J. Chem. Phys.* **2010**, *132*, No. 154104.
(35) Mathew, K.; Kolluru, V. S. C.; Mula, S.; Steinmann, S. N.; Hennig, R. G. Implicit self-consistent electrolyte model in plane-wave density-functional theory. *J. Chem. Phys.* **2019**, *151*, No. 234101.
(36) Nørskov, J. K.; Bligaard, T.; Logadottir, A.; Kitchin, J. R.; Chen, J. G.; Pandelov, S.; Norskov, J. K. Trends in the exchange current for hydrogen evolution. *J. Electrochem. Soc.* **2005**, *152*, J23−J26.
(37) Zhang, W.; Saraei, N.; Nie, H.; Vaughn, J. R.; Jones, A. S.; Mashuta, M. S.; Buchanan, R. M.; Grapperhaus, C. A. Reversible methanol addition to copper Schiff base complexes: a kinetic, structural and spectroscopic study of reactions at azomethine C=N bonds. *Dalton Trans.* **2016**, *45*, 15791−15799.
(38) Kim, D.; Shi, J.; Liu, Y. Substantial Impact of Charge on Electrochemical Reactions of Two-Dimensional Materials. *J. Am. Chem. Soc.* **2018**, *140*, 9127−9131.
(39) Zhao, X.; Liu, Y. Unveiling the Active Structure of Single Nickel Atom Catalysis: Critical Roles of Charge Capacity and Hydrogen Bonding. *J. Am. Chem. Soc.* **2020**, *142*, 5773−5777.
(40) Chen, J.-W.; Zhang, Z.; Yan, H.-M.; Xia, G.-J.; Cao, H.; Wang, Y.-G. Pseudo-adsorption and long-range redox coupling during oxygen reduction reaction on single atom electrocatalyst. *Nat. Commun.* **2022**, *13*, No. 1734.
(41) McCaffrey, D. L.; Nguyen, S. C.; Cox, S. J.; Weller, H.; Alivisatos, A. P.; Geissler, P. L.; Saykally, R. J. Mechanism of ion adsorption to aqueous interfaces: Graphene/water vs. air/water *Proc. Natl. Acad. Sci.* 2017, *114*51 13369−13373 DOI: 10.1073/pnas.1702760114.
(42) Liu, J.-C.; Xiao, H.; Li, J. Constructing High-Loading Single-Atom/Cluster Catalysts via an Electrochemical Potential Window Strategy. *J. Am. Chem. Soc.* **2020**, *142*, 3375−3383.
(43) Liu, X.; Jiao, Y.; Zheng, Y.; Jaroniec, M.; Qiao, S.-Z. Building Up a Picture of the Electrocatalytic Nitrogen Reduction Activity of Transition Metal Single-Atom Catalysts. *J. Am. Chem. Soc.* **2019**, *141*, 9664−9672.
(44) Zhu, M.; Song, W.; Konze, P. M.; Li, T.; Gault, B.; Chen, X.; Shen, J.; Lv, S.; Song, Z.; Wuttig, M.; Dronskowski, R. Direct atomic insight into the role of dopants in phase-change materials. *Nat. Commun.* **2019**, *10*, No. 3525.
(45) Bai, X.; Li, Q.; Shi, L.; Niu, X.; Ling, C.; Wang, J. Hybrid Cu^0 and Cu^{x+} as Atomic Interfaces Promote High-Selectivity Conversion of CO_2 to C_2H_5OH at Low Potential. *Small* **2020**, *16*, No. 1901981.
(46) Zhao, X.; Shi, J.; Ji, Y.; Liu, Y. The electronic structure underlying electrocatalysis of two-dimensional materials. *Wiley Interdiscip. Rev.: Comput. Mol. Sci.* **2019**, *9*, No. e1418.
(47) Mu, S.; Lu, H.; Wu, Q.; Li, L.; Zhao, R.; Long, C.; Cui, C. Hydroxyl radicals dominate reoxidation of oxide-derived Cu in electrochemical CO_2 reduction. *Nat. Commun.* **2022**, *13*, No. 3694.
(48) Vavra, J.; Shen, T.-H.; Stoian, D.; Tileli, V.; Buonsanti, R. Real-time Monitoring Reveals Dissolution/Redeposition Mechanism in Copper Nanocatalysts during the Initial Stages of the CO_2 Reduction Reaction. *Angew. Chem.* **2021**, *133*, 1367−1374.
(49) Lee, S. H.; Lin, J. C.; Farmand, M.; Landers, A. T.; Feaster, J. T.; Aviles Acosta, J. E.; Beeman, J. W.; Ye, Y.; Yano, J.; Mehta, A.; et al. Oxidation State and Surface Reconstruction of Cu under CO_2 Reduction Conditions from In Situ X-ray Characterization. *J. Am. Chem. Soc.* **2021**, *143*, 588−592.
(50) Grosse, P.; Yoon, A.; Rettenmaier, C.; Herzog, A.; Chee, S. W.; Roldan Cuenya, B. Dynamic transformation of cubic copper catalysts during CO_2 electroreduction and its impact on catalytic selectivity. *Nat. Commun.* **2021**, *12*, No. 6736.